Neural Network–Based Prediction of Wrinkling Severity in Flax Fabrics using Material and Formed-Surface Texture Parameters

O. H. Margoto[1], M. A. Batouei[1], V. Yang[1], Y. Abdin[2, *] and A. S. Milani[1, *]

[1] School of Engineering, University of British Columbia, Kelowna, Canada, [2] Department of Materials Engineering, University of British Columbia, Vancouver, Canada

* *Corresponding authors (yasmine.abdin@ubc.ca, abbas.milani@ubc.ca)*

Keywords: *Flax woven fabrics; forming-induced defect; composites reinforcements; machine learning; Haralick texture features*

1. Abstract

The forming of fabric-reinforced composites is a critical step in manufacturing lightweight, high-strength automotive and aerospace components. Poorly optimized forming conditions can lead to defects such as wrinkles, tow buckling, and in-plane waviness, which are further exacerbated in natural fibre-reinforced composites due to material variability, heterogeneous yarn structures, and porosity. This study develops a neural network–based framework for rapid prediction of forming-induced defects in flax fabric reinforcements, using a commercial glass fabric as a reference. The model combines experimentally measured mechanical properties (shear, bending, tensile, and friction) with key fabric parameters (weave type, orientation, layers, grammage, and thickness). Post-forming morphologies were obtained via high-resolution 3D scanning and converted into grayscale height maps, from which Haralick texture features were extracted and used with mechanical inputs to train a supervised neural network. The SHAP sensitivity analysis quantified feature importance, and the model robustness was evaluated using k-fold and Monte Carlo cross-validation. Results showed that fabric orientation, shear stiffness and bending stiffness are among the most influential parameters. Among the Haralick features, the dissimilarity index was most informative, with higher values indicating greater surface variation and defect severity, enabling comparison across materials. It also captured the fabric architecture effects, showing lower values for glass fibre and higher values for biaxial non-crimp flax reinforcement, and achieved the highest prediction accuracy among the test sets ($R^2 = 0.79$ for 5-fold and 0.77 for 10 Monte Carlo runs).

2. Introduction

Textile-based reinforcements are widely used in high-performance composites due to their high strength, low weight, and good formability [1]. Woven fabrics, with fibres interlaced in two directions (warp and weft), exhibit superior in-plane mechanical behavior and shear performance compared to unidirectional fibres, while Non-Crimp Fabrics (NCFs) provide higher flexibility for complex geometries [2]. Reinforcements can be synthetic, such as glass and carbon fibres, or natural, including flax, hemp, and jute. Natural fibres have gained increased interest due to their lower density and reduced energy requirements during production, with flax fibres standing out for its high strength- and stiffness-to-density ratios [3].

During forming, fabrics undergo in-plane shear, biaxial extension, inter-ply and tool–ply friction, and out-of-plane bending, which dominate the material's ability to conform to complex tool geometries [1]. Sharp corners, as in square-box tools, exacerbate wrinkling, while cylindrical tools distribute deformation more evenly [4]. Defects such as out-of-plane wrinkles, folds, and bridging, as well as in-plane yarn slippage, compromise the quality and mechanical performance of composite parts, reducing strength by up to 70% in severe cases [5].

The manufacturing and fibre architecture significantly influence formability and defect formation of composite reinforcements under complex geometries. Natural fibres, such as flax, are often composed of short, segmented fibres bonded into flat yarns or twisted yarns, affecting bending stiffness and susceptibility to tow buckling [6], [7]. Woven fabrics allow larger in-plane shear deformation, whereas NCFs' formability depends on its stitch pattern [8]. Physical parameters, including areal weight, fibre distribution and orientation, also affect preforming behavior, with higher-density fabrics generally performing better [9].

Machine Learning (ML) offers a promising alternative to traditional trial-and-error or simulation-based methods for predicting and mitigating the drapability behavior of composite materials. ML models, including Artificial Neural Networks (ANNs) [10], reinforcement learning [11], and convolutional neural networks [12], have been successfully applied to synthetic fibre-reinforced composites for defect classification, parameter optimization, and real-time process control. However, similar data-driven studies for natural fibre woven reinforcements remain scarce, despite their growing interest for sustainable composites.

This study addresses this emerging trend by developing a supervised ML framework to predict forming induced defects in commercial flax fabric reinforcements, using a glass fabric as control. Fabric physical parameters and experimentally measured mechanical properties are used as model inputs, while forming-induced defect descriptors are used as outputs. These descriptors are extracted from high-resolution 3D wrinkle maps obtained experimentally using a custom forming set-up and quantified via Haralick texture features. Formability is predicted using an ANN, feature importance is analyzed using SHapley Additive exPlanations (SHAP), and the model robustness is evaluated using both k-fold and Monte Carlo cross validation methods.

3. Methodology

Three commercial flax fabrics and a glass fabric (as a control) were selected. FTW250 and FTW367 are 2x2 twill flax fabrics with tow orientations of 0/90°, areal weights of 250 and 367 g/m² and thicknesses of 0.78 and 1.29 mm, respectively, both from Lingrove (US). FBX350 is a ±45° biaxial non-crimp flax fabric with areal weight of 350 g/m² and a thickness of 0.97 mm, manufactured by Bcomp Ltd. (CH). The glass fabric, GTW280, is a 2x2 twill with 0/90° tow orientation, areal weight of 280 g/m² and a thickness of 0.29 mm from Easy Composites (UK). Figure 1 summarizes the methodology used in this study, as per authors' previous work [13].

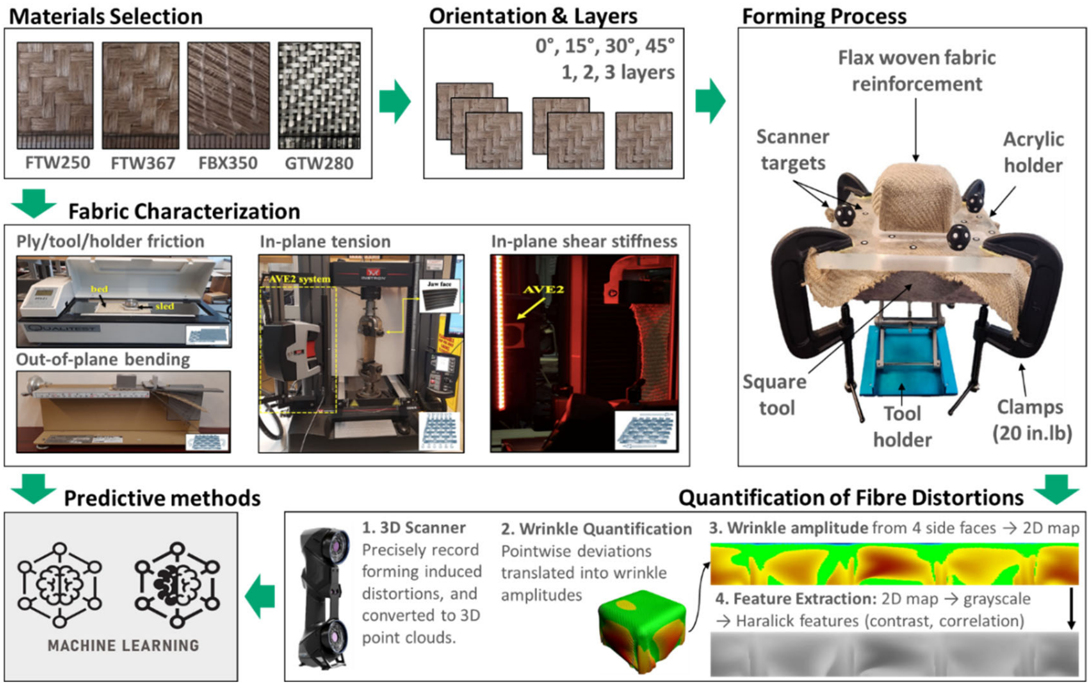

Figure 1: Workflow for predicting fabric formability, showing the sequence from material selection and mechanical testing to 3D forming using a custom set-up, data collection, and extraction of Haralick features for neural network modeling [13].

A customized 3D forming setup was used to evaluate the forming behavior of the fabrics, consisting of a 112 mm square-box tool and a 25.4 cm thick acrylic fabric holder. Fabric specimens (45 × 45 cm) were cut at predefined fibre orientations (0°, 15°, 30°, 45°) and layer configurations (1–3 layers), draped manually over the tool, and clamped under controlled torque. Surface geometries and forming-induced defects were captured using a Handyscan Black Elite 3D scanner (Creaform Inc., CA) with 0.025 mm accuracy.

3.1. Quantification of Fibre Distortions

The post-forming morphologies obtained via 3D scanning were saved as point clouds and processed in Python. The surfaces were converted to polar coordinates relative to the tool center, and forming-induced deformations were quantified by subtracting the radial distance of the respective scanned surface from that of the nominal square-box tool geometry. This approach produced a one-dimensional deformation profile capturing local out-of-plane surface deviations during forming. Next, to further characterize deformations on the lateral surfaces, two-dimensional maps were generated by unfolding the vertical faces of the formed box into grayscale images, where pixel intensity represents the magnitude of deviations. The top surface was excluded, as defect formation in this region was negligible for most samples and thus contributed limited information for distinguishing forming outcomes. Each scanned surface map was then analyzed using Gray Level Co-Occurrence Matrices (GLCM), from which normalized Haralick features, including contrast and dissimilarity were extracted [14]. The full experimental and computational procedure has been described in detail in the authors' previous work [13].

3.2. Fabric Mechanical characterization

The mechanical behavior of the FTW250, FTW367, FBX350 and GTW280 reinforcements, including ply-tool friction, out-of-plane bending, in-plane tension, and in-plane shear, was characterized in the authors' previous work [13], [15] to capture the deformations occurring during complex 3D forming. The summary of their properties is presented in Table 1 below.

Table 1: Mechanical properties of the tested fabric reinforcements at 0/90° orientation [13].

Fabric (type)	$\downarrow$ **Young's Modulus (GPa)**	$\downarrow$ **Shear Stiffness at 40° ($N.mm^{-1}$)**	$\uparrow$ **Bending Stiffness (N.mm)**	$\downarrow$ **Ply-tool Friction Coefficient**
FTW250	0.24 ± 0.08	0.008 ± 0.001	1.47 ± 0.16	0.17 ± 0.00
FTW367	0.46 ± 0.11	0.021 ± 0.002	1.61 ± 0.47	0.16 ± 0.00
FBX350	0.57 ± 0.15	0.069 ± 0.035	1.04 ± 0.09	0.15 ± 0.00
GTW280	3.29 ± 0.34	0.012 ± 0.002	0.07 ± 0.01	0.22 ± 0.01

* Arrows indicate literature-supported trends associated with reduced forming-induced wrinkles [1], [4].

Following the study [16], the effective out-of-plane bending stiffness D_{eff} for each predefined fibre orientation (0°, 15°, 30°, 45°) was calculated following from the measured flexural rigidity D using:

$$D_{eff} = D \cos^2 \theta \tag{1}$$

where θ is the fabric angle measured relative to the tool square corner.

The effective modulus E_{eff} for each fabric orientation was calculated from the initial linear region of the stress–strain curve [17], [18] as per Eq. 2:

$$E_{eff} = (\cos^4 \theta + \sin^4 \theta) \tag{2}$$

where E is the effective in-plane modulus in the loading direction, and θ is the fibre orientation relative to the load [17], [18]. Shear stiffness was measured via bias extension tests with specimens oriented at 45° to the fibre direction, and the shear modulus was taken at a typical high value of 40° shear angle, consistent with [4].

3.3. Artificial Neural Network for Wrinkling Severity Prediction

To predict the severity of forming-induced defects in composite reinforcements, Haralick texture features such as contrast and dissimilarity were used as target outputs. The dataset comprised 48 samples from four commercial fabric reinforcements (FBX350, FTW250, FTW367, and GTW280). Key fabric parameters (orientation, number of layers, grammage, and thickness), together with fabric mechanical properties (Table 1), were used as input variables to an artificial neural network model. A separate ANN was developed for each Haralick texture feature, each consisting of eight input variables, two hidden layers with eight neurons each, and a single output node. The data were randomly split into 56% for training, 14% for validation, and 30% for testing. Model training employed early stopping, terminating after 600 consecutive iterations without improvement in validation loss.

SHAP was used to interpret the ANN results by quantifying the contribution of each input feature to the model predictions, using all available training set as the background dataset. To assess model robustness and generalization, both 5-fold cross-validation and Monte Carlo cross-validation performed. In 5-fold cross-validation, each sample is included exactly once in the validation set, ensuring complete coverage [19]. Monte Carlo cross-validation uses 10 random splits, so while samples may appear in multiple validation sets, it is also possible that some samples are not included in the validation set in certain runs, providing a stochastic estimate of the model performance [20].

4. Results and Discussion

Post-forming morphologies were obtained via high-resolution 3D scanning and subsequently represented as 2D deformation heat maps, as shown in Figure 2. In these maps, the color scale reflects the magnitude and nature of out-of-plane deformation: red indicates regions of high out-of-plane deformation, while yellow correspond to progressively lower wrinkle amplitudes. Green regions represent areas within a ±2 mm deformation range, which is considered acceptable in terms of forming quality in this study. In contrast, blue regions (below -2 mm) indicate negative out-of-plane deviations, mainly associated with local compaction and/or buckling during the forming process.

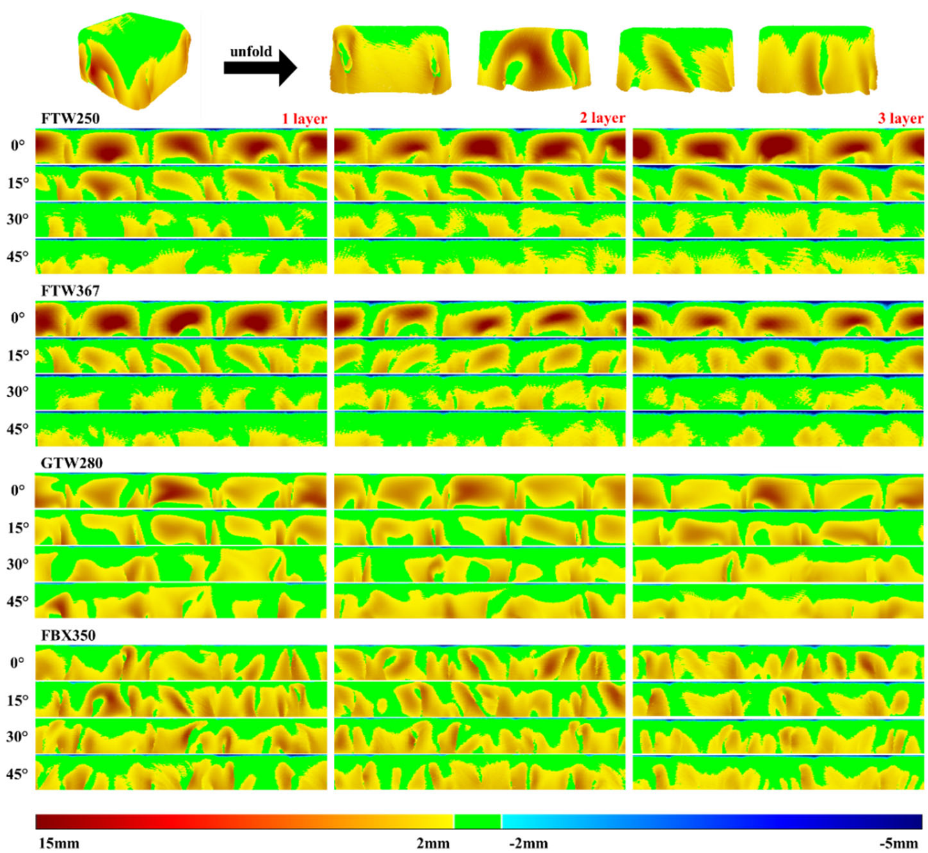

Figure 2: Post-forming morphologies visualized as 2D deformation heat maps from high-resolution 3D scans. Note that for the multi-layer configurations, the maps show the outer layer deformation.

As observed in Figure 2, the deformation behavior of formed parts varies significantly with material architecture, fabric orientation, and number of layers, revealing not only differences in deformation magnitude but also distinct wrinkle morphologies. In addition, corner regions consistently exhibited localized zones of high deformation, visible as concentrated wrinkle clusters (red) or compressed regions (blue), reflecting the combined effects of geometric constraints and material compaction that promote localized instabilities.

In the single-layer configuration, the woven reinforcements (FTW250, FTW367, and GTW280) exhibited their most pronounced defects at 0°, characterized by bulky and highly pronounced wrinkle regions spanning multiple faces of the geometry in the flax reinforcements, and less intense deformation patterns for the glass reinforcement. These wrinkles appeared as broad undulations, indicating that deformation was accommodated through global out-of-plane bending rather than localized instabilities. Although the FBX350 NCF reached comparable deformation magnitudes, it exhibited a distinct morphology with isolated folding zones and sharp transitions, with its poorest performance at 15°.

As the fabric orientation increased from 0° to 45°, a clear transition in wrinkle morphology was observed for the woven reinforcements, particularly FTW250 and FTW367. At 30° and 45°, the deformation patterns evolved into finer, lower-amplitude wrinkles that were more diffuse and less spatially continuous. FTW367 showed the most pronounced improvement, resulting in smoother overall surfaces attributed to the reduced tensile constraint (as defined in Eq. 2) and the increased ability of the reinforcement to undergo in-plane shear, particularly at the sharp edges of the box tool where double curvature is imposed. This enables fabric deformation to be accommodated through yarn rotation rather than in-plane compression, thereby limiting compression-driven wrinkling. In addition, the effective bending response of the woven reinforcements at 45° is lower than at 0°, reducing resistance to out-of-plane deformation and promoting more diffuse wrinkle patterns [16]. In contrast, FBX350 exhibited relatively unchanged deformation patterns across different orientations, with similar localized folds. This behavior is attributed to its higher in-plane shear stiffness (Table 1) and restricted yarn mobility due to the stitch architecture, which limit its ability to adapt to complex deformation modes [8].

The transition from single-layer to three-layer configurations did not lead to a pronounced change in wrinkle morphology. For most materials, the overall deformation pattern remained similar, with only a slight increase in localized out-of-plane deviations in the scanned outer layer. This effect was more noticeable for FTW250 and FTW367, where the respective three-layer configurations exhibited a greater extent of negative out-of-plane deviations (blue regions evident at the top of the 2D maps shown in Figure 2, corresponding to the corner regions of the square-tool), which were associated with increased local compaction and/or buckling during forming compared to single-layer configurations. GTW280, on the other hand, showed the least change in deformation morphology with additional layers, maintaining very similar patterns across all configurations. These observations can be associated with inter-ply friction effects, which become more pronounced in thicker flax fabric multi-layer configurations due to higher inter-layer contact pressure compared to GTW280, which has the lowest nominal thickness per layer in this study.

The resulting through-thickness compaction in thicker layout configurations may further restrict ply mobility through increased inter-ply frictional interaction during forming [1].

Next, grayscale height maps extracted from the deformation maps (Figure 2) were used to compute Haralick texture features, which served as inputs to the ANN models. Separate models were developed for each selected Haralick feature to represent post-forming wrinkling severity. The ANN models' predictions were further interpreted using SHAP analysis to identify the factors most influencing wrinkling severity. The results confirmed that fabric effective bending stiffness, shear stiffness, and orientation had the largest impact on predicted wrinkle severity among the tested materials and configurations. This aligns with the observations from Figure 2, where variations in wrinkle morphology were most pronounced at higher fabric orientations and were strongly influenced by the fabric's bending and shear response, consistent with [1], [4], [8], [16].

Figure 3 and Table 2 summarize the ANN models' performance in terms of R^2 and Mean Absolute Error (MAE) over 5 k-fold and 10 Monte Carlo cross-validation runs, illustrating both the accuracy and stability of the models under repeated resampling.

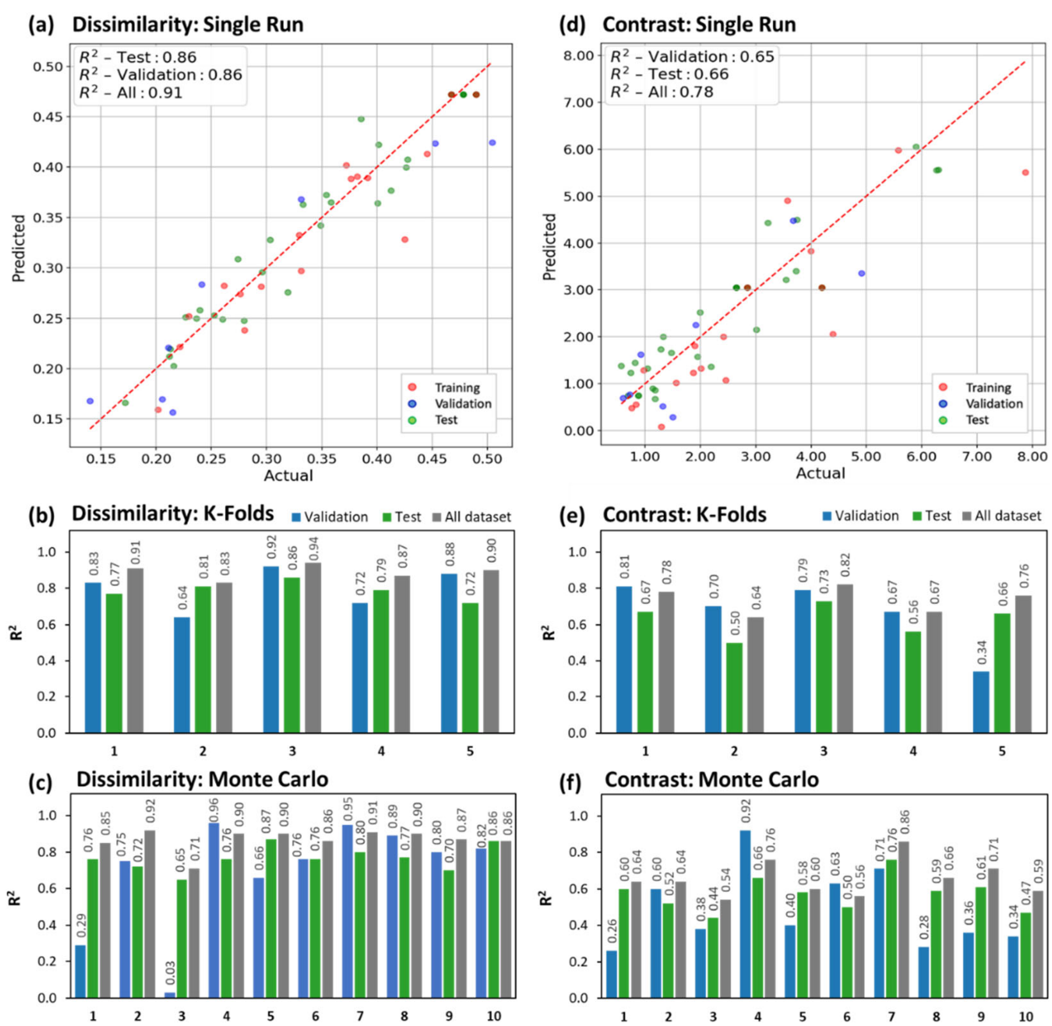

Figure 3: ANN predictions using Haralick features: Dissimilarity (left) and Contrast (right). Graphs show (a,d) actual vs. predicted, (b,e) k-fold R^2 per iteration, and (c,f) Monte Carlo R^2 per iteration.

Table 2: Mean ± standard deviation performance of ANN models obtained across k-fold and Monte Carlo cross-validation runs for the prediction of the Haralick texture features contrast and dissimilarity (dependent variables).

	Haralick Features (ML Output)		Contrast	Dissimilarity
K-fold	R-square (R^2)	Validation	0.66 ± 0.19	0.80 ± 0.12
		Test	0.63 ± 0.09	0.79 ± 0.05
		All dataset	0.73 ± 0.07	0.89 ± 0.04
	Mean Absolute Error (MAE)	Validation	0.69 ± 0.14	0.03 ± 0.01
		Test	0.82 ± 0.14	0.03 ± 0.00
		All dataset	0.64 ± 0.11	0.02 ± 0.01
Monte Carlo	R-square (R^2)	Validation	0.49 ± 0.22	0.69 ± 0.30
		Test	0.57 ± 0.10	0.77 ± 0.07
		All dataset	0.66 ± 0.10	0.87 ± 0.06
	Mean Absolute Error (MAE)	Validation	0.69 ± 0.30	0.03 ± 0.01
		Test	0.87 ± 0.10	0.03 ± 0.00
		All dataset	0.73 ± 0.13	0.03 ± 0.01

Among the evaluated Haralick texture features, the ANN model achieved its predicted most accurately prediction for the dissimilarity index, with a k-fold–averaged testing R^2 of up to 0.79, as shown in Figure 3 and Table 2. The dissimilarity index is known to capture the intensity difference between each pixel and its neighbors, reflecting local variations in gray levels [21], [22]. In the context of this study, higher dissimilarity values indicate greater texture variation, corresponding to more severe surface defects. Accurate prediction of dissimilarity thus enabled quantitative comparison of wrinkle severity across different materials. This feature also reflected differences in fabric architecture: glass fibre reinforcement exhibited lower dissimilarity values, while FBX350 showed higher values. Across all sample configurations and cross-validation runs, including training, validation, and testing sets, the dissimilarity index consistently yielded reliable predictions, with a minimum R^2 of 0.69.

When analyzing the contrast index, the test R^2 of 0.63 indicated some potential for this Haralick feature to represent wrinkle severity. However, the relatively high MAE observed across both cross-validation methods suggests that the model predictions were inconsistent. This behavior is likely related to the limited dataset used in this study (48 samples) and the complexity of the ANN, which may have prevented the model from capturing contrast patterns that generalize effectively. Future work could address this limitation by increasing the dataset size or employing a less 'data-hungry' machine learning approach [23] to further evaluate the predictive potential of this Haralick texture feature.

5. Conclusions

In this study, post-forming surface deformations were quantified using high-resolution 3D scanning, and Haralick texture features were extracted as quantitative descriptors of defect severity. A neural network trained on fabric mechanical properties and forming parameters was then used to predict these features for flax and glass fabric reinforcements. The results showed that the dissimilarity index provided the most reliable predictions, effectively capturing both defect severity and fabric architecture effects. More specifically, the ANN models achieved average testing R^2 values of 0.79 for k-fold cross-validation and 0.76 for Monte Carlo cross-validation when using the dissimilarity index as a measure of wrinkle severity. Another Haralick feature, contrast, was also used to train ANN model; however, it showed moderate predictive capability, with R^2 values of 0.63 and 0.57, respectively, along with higher MAE. SHAP analysis further revealed that effective bending stiffness, shear stiffness, and fabric orientation are the dominant factors governing wrinkle formation and defect severity across materials and orientations.

Despite these promising results, the study is limited by a small dataset (48 samples), a restricted range of reinforcement types, and the use of a single box-shaped geometry, which may reduce model generalizability. Future work should therefore expand the dataset to include additional natural and synthetic reinforcements, investigate alternative tool geometries to capture more complex deformation modes, and evaluate a broader range of Haralick features or alternative texture descriptors to enhance defect characterization. Machine learning approaches with lower data requirements and reduced model complexity may also be explored to enhance prediction stability. These efforts may ultimately contribute to improved predictive accuracy and robustness of data-driven frameworks for optimizing composite forming processes.

6. References

[1] Armin Rashidi Mehrabadi, "Towards mitigation of wrinkles during forming of woven fabric composites: an experimental characterization," University of British Columbia, 2016.

[2] E. Marklund, L. E. Asp, and R. Olsson, "Transverse strength of unidirectional non-crimp fabric composites: Multiscale modelling," *Compos. B Eng.*, vol. 65, pp. 47–56, 2014.

[3] Ankit, M. Rinawa, P. Chauhan, D.Suresh, S. Kumar, and R. Santhosh Kumar, "A review on mechanical properties of natural fiber reinforced polymer (NFRP) composites," *Mater. Today Proc.*, 2021.

[4] R. Bai, B. Chen, J. Colmars, and P. Boisse, "Physics-based evaluation of the drapability of textile composite reinforcements," *Compos. B Eng.*, vol. 242, pp. 1–15, 2022.

[5] K. Potter, B. Khan, M. Wisnom, T. Bell, and J. Stevens, "Variability, fibre waviness and misalignment in the determination of the properties of composite materials and structures," *Compos. Part A Appl. Sci. Manuf.*, vol. 39, pp. 1343–1354, 2008.

[6] P. Ouagne, D. Soulat, J. Moothoo, E. Capelle, and S. Gueret, "Complex shape forming of a flax woven fabric; analysis of the tow buckling and misalignment defect," *Composites Part A*, vol. 51, pp. 1–10, 2013.

[7] P. Ouagne et al., "Use of bast fibres including flax fibres for high challenge technical textile applications. Extraction, preparation and requirements for the manufacturing of composite reinforcement fabrics and for geotextiles," in Handbook of Natural Fibres, Elsevier Ltd, 2020, pp. 169–204.

[8] Y. M. Fei, "The Prediction of Wrinkle Formation in Non-crimp Fabrics during Double Diaphragm Forming," Master, University of Nottingham, 2021.

[9] F. Omrani, P. Wang, D. Soulat, M. Ferreira, and P. Ouagne, "Analysis of the deformability of flax-fibre nonwoven fabrics during manufacturing," *Compos. B Eng.*, vol. 116, pp. 471–485, 2017.

[10] L. Bin Tan and N. D. P. Nhat, "Prediction and Optimization of Process Parameters for Composite Thermoforming Using a Machine Learning Approach," *Polymers (Basel).*, vol. 14, no. 14, 2022.

[11] C. Zimmerling, C. Poppe, O. Stein, and L. Kärger, "Optimisation of manufacturing process parameters for variable component geometries using reinforcement learning," *Mater. Des.*, vol. 214, p. 110423, 2022.

[12] A. Djavadifar, J. B. Graham-Knight, M. Körber, P. Lasserre, and H. Najjaran, "Automated visual detection of geometrical defects in composite manufacturing processes using deep convolutional neural networks," *J. Intell. Manuf.*, vol. 33, no. 8, pp. 2257–2275, 2022.

[13] O. H. Margoto, M. A. Batouei, V. Yang, Y. Abdin, and A. S. Milani, "Machine Learning-Based Prediction of Forming-Induced Defects in Flax Woven Fabrics Using 3D Scanning and Haralick Texture Features," in *Materials Science Forum*, Thessaloniki: Trans Tech Publications Ltd, Apr. 2026, pp. 59–71.

[14] Y. Park and J. M. Guldmann, "Measuring continuous landscape patterns with Gray-Level Co-Occurrence Matrix (GLCM) indices: An alternative to patch metrics?," *Ecol. Indic.*, vol. 109, 2020.

[15] O. H. Margoto, A. Nazemi, Y. Abdin, and A. S. Milani, "On drapability and characterization of flax fabric reinforcements," in International SAMPE Technical Conference, Soc. for the Advancement of Material and Process Engineering, 2024.

[16] R. Sourki, B. Crawford, R. Vaziri, and A. S. Milani, "Meso-level bending/reverse-bending analysis of dry woven fabrics: Observing an irreversible behavior during forming," *Compos. Struct.*, vol. 282, 2022.

[17] X. Q. Peng and J. Cao, "A continuum mechanics-based non-orthogonal constitutive model for woven composite fabrics," *Compos. Part A Appl. Sci. Manuf.*, vol. 36, no. 6, pp. 859–874, 2005.

[18] A. Gasser, P. Boisse, and S. Hanklar, "Mechanical behaviour of dry fabric reinforcements. 3D simulations versus biaxial tests," *Comput. Mater. Sci.*, vol. 17, pp. 7–20, 2000.

[19] F. Kjeldsberg, Z. H. Munim, M. Bustgaard, S. Bhagat, E. Lindroos, and P. Haavardtun, "Sensitivity of Predictive Performance Assessment Accuracy in Varying k-fold Cross Validation," pp. 71–82, 2025.

[20] G. Shan, "Monte Carlo cross-validation for a study with binary outcome and limited sample size," *BMC Med. Inform. Decis. Mak.*, vol. 22, no. 1, 2022.

[21] I. Vrbik et al., "Haralick texture feature analysis for quantifying radiation response heterogeneity in murine models observed using Raman spectroscopic mapping," *PLoS One*, vol. 14, no. 2, 2019.

[22] D. L. Campbell, H. Kang, and S. Shokouhi, "Application of haralick texture features in brain [18F]-florbetapir positron emission tomography without reference region normalization," *Clin. Interv. Aging*, vol. 12, pp. 2077–2086, 2017.

[23] D. Sarkar, M. Ramezankhani, A. Narayan, and A. S. Milani, "Non data hungry smart composite manufacturing using active transfer learning with sigma point sampling (SPSATL)," Comput. Ind., vol. 151, 2023.